論文 / 著書情報
Article / Book Information

Title	Analysis and control of the Hanle effect in metal–oxide–semiconductor inversion channels
Authors	Y. Takamura, S. Sugahara
Citation	J. Appl. Phys., vol. 111, Issue 7, pp. 07C323/1-3
Pub. date	2012, 3
Note	This article may be downloaded for personal use only. Any other use requires prior permission of the author and AIP Publishing. The following article appeared in J. Appl. Phys., vol. 111, Issue 7, pp. 07C323/1-3 and may be found at http://dx.doi.org/10.1063/1.3680534.

AIP Journal of Applied Physics

Analysis and control of the Hanle effect in metal–oxide–semiconductor inversion channels

Yota Takamura and Satoshi Sugahara

Citation: J. Appl. Phys. **111**, 07C323 (2012); doi: 10.1063/1.3680534
View online: http://dx.doi.org/10.1063/1.3680534
View Table of Contents: http://jap.aip.org/resource/1/JAPIAU/v111/i7
Published by the AIP Publishing LLC.

Analysis and control of the Hanle effect in metal–oxide–semiconductor inversion channels

Yota Takamura[1,2,a)] and Satoshi Sugahara[1,2,3,b)]
[1]*Department of Electronics and Applied Physics, Tokyo Institute of Technology, Yokohama 226-8503, Japan*
[2]*Imaging Science and Engineering Laboratory, Tokyo Institute of Technology, Yokohama 226-8503, Japan*
[3]*CREST, Japan Science and Technology Agency, Kawaguchi 332-0012, Japan*

(Presented 3 November 2011; received 30 September 2011; accepted 3 January 2012; published online 14 March 2012)

The authors theoretically analyzed the output characteristics of a proposed Hanle-effect spin transistor based on a spin-MOSFET. The device can easily create oscillating Hanle-effect signals by applying an accelerating bias voltage. The behavior of the magnetic field interval of the oscillatory Hanle-effect signals for a sufficiently high accelerating bias is well correlated with the universality of the effective electron mobility in the Si MOS inversion channel, which is useful for revealing spin transport dynamics in the MOS inversion channel. © *2012 American Institute of Physics*. [doi:10.1063/1.3680534]

In recent years spin-functional MOSFETs (spin MOSFETs)[1–4] have attracted considerable attention for future low-power logic circuits[5,6] owing to their unique spin-dependent transistor characteristics. Understanding and controlling spin injection/transport/detection for Si MOS inversion channels are critical challenges for realizing spin-functional MOSFETs. The Hanle effect induced by the spin precession of traveling spin-polarized electrons in semiconductor channels[7–10] is considered to be the most powerful tool for investigations of the spin transport phenomena. The spin dynamics (e.g., spin lifetime) can be analyzed quantitatively from the magnetic field interval (which is referred to as $B_\pi^{\rm osc}$ in this paper) between the oscillation peaks of Hanle-effect signals.[7–10] The spin accumulation technique using three terminal devices[11,13] has widely been employed to investigate the Hanle effect. However, this technique cannot distinguish observed signals from other spurious signals such as spin signals from trapped electrons at the ferromagnet–semiconductor interface.[14] Furthermore, spin transport phenomena in the semiconductor channel cannot be evaluated with this technique. The nonlocal technique using four terminal devices[12,15] can evaluate the Hanle effect for pure spin currents in the semiconductor channel. However, its signal intensities are weak, and multiple oscillations cannot be obtained owing to the diffusive spin transport that causes the strong dephase effect.

Recently we proposed a novel Hanle-effect spin transistor based on a spin-MOSFET shown in Fig. 1.[16] The detailed operation principle was described in Ref. 16. The device has the ability to detect oscillatory Hanle-effect signals with high sensitivity and to distinguish spin transport signals from other spurious signals, since multiple oscillating Hanle-effect signals can easily be created in the device using the drift transport mechanism. Furthermore, we found that the Hanle-effect signals are well correlated with the universality[17] of the effective electron mobility $\mu_{\rm eff}$ in the MOS inversion channel. Note that although the carrier density in the MOS inversion channel could be important for this feature, it can be controlled by not only a gate bias but also a body (substrate) bias (not shown in Fig. 1). In this paper, we analyze the Hanle effect in the proposed spin transistor. The behavior of $B_\pi^{\rm osc}$ is shown to obey the universality of the effective electron mobility in the MOS inversion channel, which is useful for investigating the spin transport dynamics in the MOS inversion channel.

The magnetotransport properties of the Hanle-effect spin transistor were analyzed using the rate equation of spin-polarized electrons,[16]

$$\frac{\partial s(x,t)}{\partial t} = D\frac{\partial^2 s(x,t)}{\partial x^2} - v\frac{\partial s(x,t)}{\partial x} - \frac{s(x,t)}{\tau_{\rm sf}}, \qquad (1)$$

where $s(x, t)$ is the spin density, D is the diffusion constant, v is the velocity, and $\tau_{\rm sf}$ is the spin lifetime. The spin density s is defined by $n_\uparrow - n_\downarrow$ using a spin-up electron density $n_\uparrow$ and a spin-down electron density $n_\downarrow$, and the total electron density n can be given by $n_\uparrow + n_\downarrow$. In this study, s and n were measured as normalized values for simplicity. In the calculation, we assumed that a MOSFET operation in the linear region was applied to the Hanle-effect spin transistor. The spin polarization of injected electrons at the source-side channel edge was assumed to be unity in order to extract a primary physical picture. In addition, the width of the ferromagnetic contacts was assumed to be sufficiently shorter than the channel length. The impulse response of s for the time domain can easily be obtained using the Laplace

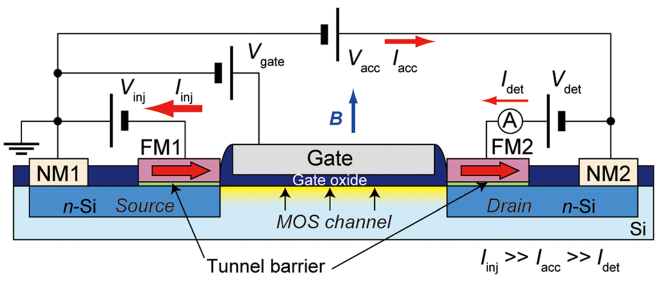

FIG. 1. (Color online) Schematic device structure of our proposed Hanle-effect spin transistor.

[a)]Electronic mail: yota@isl.titech.ac.jp.
[b)]Electronic mail: sugahara@isl.titech.ac.jp.

transform of Eq. (1) with an assumption of an infinite channel length. The effective spin polarization $P_{\mathrm{eff}}(B)$ at the drain-side channel edge can be expressed using the convolution of the impulse response with the phase factor caused by the Hanle effect.

$$P_{\mathrm{eff}}(B) = \int_0^{\infty} \frac{L}{2t\sqrt{\pi D t}} e^{-\frac{(L-vt)^2}{4Dt}} e^{-\frac{t}{\tau_{\mathrm{sf}}}} \cos\left(\frac{g\mu_B B}{\hbar} t\right) \mathrm{d}t, \quad (2)$$

where B is a magnetic field, L is the channle length, g is the g-factor ($=2$) of Si, μ_B is the Bohr magneton, and $\hbar$ is the reduced Planck constant. D was estimated from the Einstein relation using the universal effective electron mobility μ_{eff} in Si MOS inversion channels,[17] in which the correction due to the Fermi integral was ignored. The following parameters were used as a central parameter set unless otherwise noted: $L = 10\,\mu$m, $\mu_{\mathrm{eff}} = 600$ cm^2/V s (at 300 K),[17] $\tau_{\mathrm{sf}} = 8$ ns (at 300 K),[18] and operation temperature $T = 300$ K. Here, we chose the value of μ_{eff} from the phonon scattering region in the universal curve of μ_{eff} for a channel with a low doping density of 3.9×10^{15} cm^{-3} (Ref. 17). The detection current I_{det} is proportional to the effective spin polarization $P_{\mathrm{eff}}(B)$ of the transported electrons at the drain-side channel edge.

Figure 2(a) shows the impulse response of s (hereafter denoted as s_{I}) for several acceralating bias voltages V_{acc} under $B = 0$. The distribution of s_{I} sharpens with increasing V_{acc} owing to the effect of the drift transport. These sharp distribution shapes suppress the dephase effect caused by the phase factor in Eq. (2). The intensity of s_{I} increases with increasing V_{acc}, and the average transit time $t_{\mathrm{s}}^{\mathrm{ave}}$, which corresponds to the peak position of s_{I}, is shortened with increasing V_{acc}. This means that more spin-polarized electrons can reach the drain-side channel edge for higher $V_{\mathrm{acc.}}$ without randomizing the phase information. These phenomena are also confirmed by Figs. 2(b) and 2(c). The spin polarization P_{S} ($= P_{\mathrm{eff}}(0)$) is given by the ratio between the areas of s_{I} and n_{I} (which is the impulse response of n), and P_{S} is enhanced with increasing V_{acc}. Figure 2(d) shows P_{S} as a function of L for $V_{\mathrm{acc}} = 0$ to 10 V. Note that the curve for $V_{\mathrm{acc}} = 0$ corresponds to the case of a four-terminal nonlocal measurement configuration.[12,15] P_{S} decreases with increasing L; however, the effective spin diffusion length is enlarged by applying V_{acc}. Therefore, the intensity of the Hanle effect signals can be greatly enhanced relative to nonlocal measurements by the application of V_{acc}.

A magnetic field B_π required to rotate the spin direction of the transported electrons by π is given by the interval B_π^{osc} between the 1st and 2nd oscillating peaks of P_{eff}. However, its accuracy depends on whether V_{acc} is sufficient or not. Curves in Fig. 3(a) show P_{eff} as a function of B for $V_{\mathrm{acc}} = 0$ and 3 V. For the nonlocal condition (thinner curve and inset), the peak intensity at $B = 0$ is highly weakened, and the multiple oscillation is unclear because of the strong dephase effect. Although the second peaks are severely reduced, they could be detected with the use of highly sensitive measurement techniques.[13,17] However, these peaks cannot represent B_π because of the effect of the diffusive transport with the considerable spin relaxation. In contrast, when V_{acc} is sufficiently applied, P_{eff} dramatically increases and the multiple oscillations become clear, as shown by the thick curve in Fig. 3(a). In this situation, the B_π^{osc} approximately represent B_π. This is due to the dephase effect's being weakened by the application of V_{acc}, as described in Figs. 2(a)–2(c).

The relation between B_π^{osc} and the phase of the integrand of Eq. (2) at $t = t_{\mathrm{s}}^{\mathrm{ave}}$ can be expressed by the following formula:

$$\frac{g\mu_B B_\pi^{\mathrm{osc}}}{\hbar} t_{\mathrm{s}}^{\mathrm{ave}} = \pi - \theta, \quad (3)$$

where $\pi - \theta$ is the phase of the integrand of Eq. (2) at $t = t_{\mathrm{s}}^{\mathrm{ave}}$, $t_{\mathrm{s}}^{\mathrm{ave}} = t_{\mathrm{e}} - \Delta t$ [in which t_{e} is the particle picture

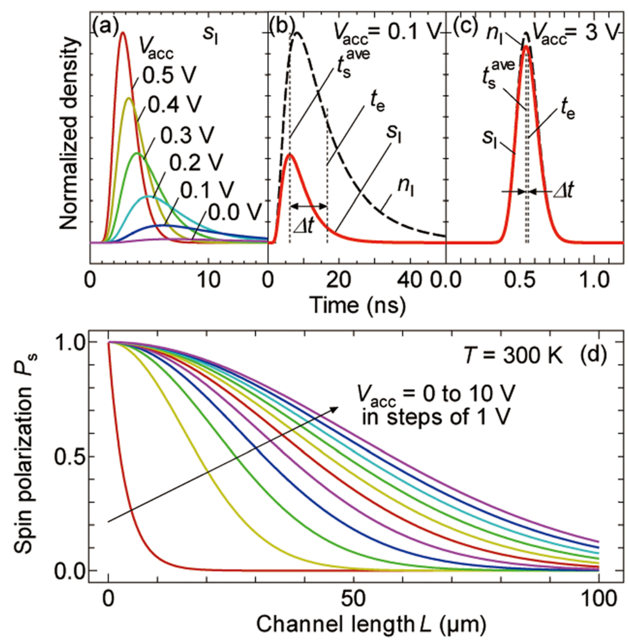

FIG. 2. (Color online) (a) Impulse response of s for $V_{\mathrm{acc}} = 0$, 0.1, 0.2, 0.3, 0.4, and 0.5 V. Impulse responses of s (solid curve) and n (dashed curve) for (b) $V_{\mathrm{acc}} = 0.1$ V and (c) $V_{\mathrm{acc}} = 3$ V are also shown. (d) P_{S} as a function of L for $V_{\mathrm{acc}} = 0$ to 10 V in steps of 1 V.

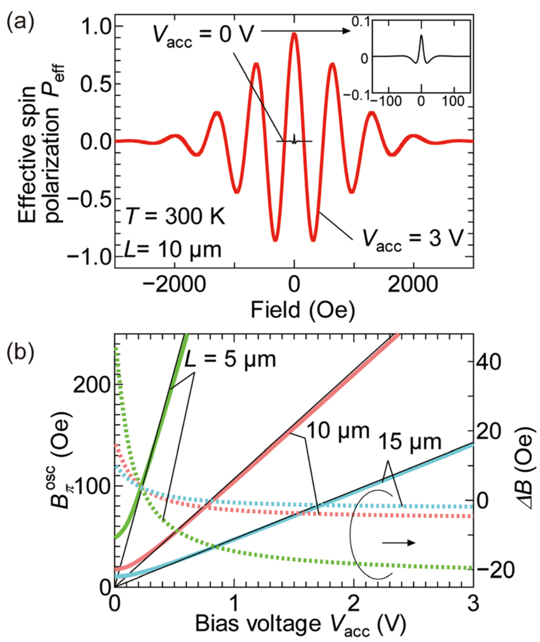

FIG. 3. (Color online) (a) P_{eff} as a function of B for $V_{\mathrm{acc}} = 0$ V (thin curve) and 3 V (thick curve). The inset shows a magnified curve for $V_{\mathrm{acc}} = 0$ V. (b) B_π^{osc} (left vertical axis) and ΔB (right vertical axis) as a function of V_{acc} for $L = 5$, 10, and 15 μm.

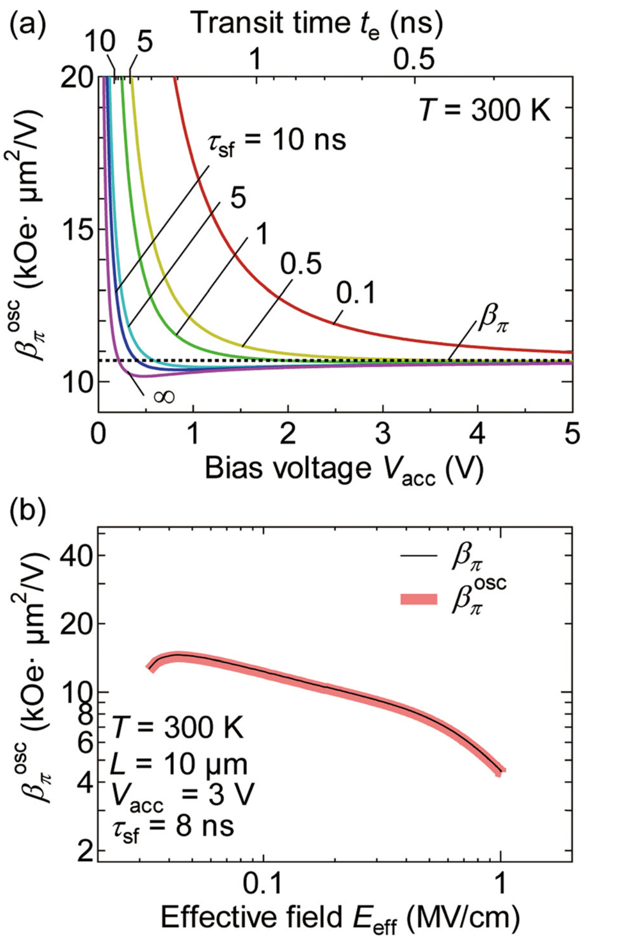

FIG. 4. (Color online) (a) β_π^{osc} as a function of V_{acc} for $E_{eff} = 0.15$ MV/cm in which τ_{sf} is varied from 0.1 to 10 ns. (b) β_π^{osc} as a function of E_{eff} for $V_{acc} = 3$ V and $\tau_{sf} = 8$ ns.

representation of the transit time given by $t_e = L/\mu_{eff}(V_{acc}/L) = L^2/\mu_{eff}V_{acc}$], and Δt (>0) is the difference between t_s^{ave} and t_e. (Δt originates from the diffusive transport with the considerable spin relaxation.) Δt depends on τ_{sf} and cannot be negligible when V_{acc} is small, as shown in Fig. 2(b). B_π^{osc} gives the phase different from π, and thus the correction factor θ is added in Eq. (3). B_π^{osc} can be expressed as

$$B_\pi^{osc} = \beta_\pi \frac{V_{acc}}{L^2} + \Delta B, \quad (4)$$

where β_π is given by $\pi\hbar\mu_{eff}/g\mu_B$ and ΔB is the correction factor due to θ and Δt. Here, β_π^{osc} is defined as $\beta_\pi^{osc} = B_\pi^{osc}L^2/V_{acc}$. When ΔB can be neglected, β_π^{osc} corresponds to β_π. The thick solid curves in Fig. 3(b) show B_π^{osc} as a function of V_{acc} for $L = 5$, 10, and 15 μm. B_π^{osc} linearly increases according to V_{acc}/L^2 (shown by the thin solid lines in Fig. 3(b)) for higher V_{acc} (Also, see Refs. 7, 8 and 16), since the drift mechanism dominates in this region. For small V_{acc}, B_π^{osc} deviates from V_{acc}/L^2, owing to the diffusive transport (in which t_s^{ave} cannot be approximated by t_e because of the considerable spin relaxation and, thus, large θ; i.e., ΔB cannot be negligible). The dotted curves in Fig. 3(b) show ΔB as a function of V_{acc}. ΔB decreases with increasing V_{acc} and tends to saturate at a constant value depending on L. Therefore, when V_{acc} is sufficiently high, ΔB can be neglected and β_π can be obtained from β_π^{osc}.

$\beta_\pi(= \pi\hbar\mu_{eff}/g\mu_B)$ is proportional to μ_{eff}, and μ_{eff} in MOS inversion channels is governed by the vertical effective electric field E_{eff} induced by a gate bias V_{gate}, which is known as the universality of μ_{eff}. β_π also shows the same universality of μ_{eff}. Figure 4(a) shows β_π^{osc} as a function of V_{acc} for $E_{eff} = 0.15$ MV/cm, in which τ_{sf} is varied from 0.1 to 10 ns. The top horizontal axis shows t_e. When t_e is sufficiently shorter than τ_{sf}, β_π^{osc} corresponds to β_π. In contrast, when t_e is longer than τ_{sf}, β_π^{osc} deviates from β_π. In order to satisfy $\beta_\pi^{osc} = \beta_\pi$, a higher V_{acc} is required for shorter τ_{sf}. These behaviors can be attributed to the V_{acc}-dependent ΔB. When a sufficiently high V_{acc} is applied so that the relation $t_e < \tau_{sf}$ is satisfied, β_π^{osc} is identical to β_π regardless of τ_{sf}.

A thick solid curve in Fig. 4(b) shows β_π^{osc} as a function of E_{eff}. β_π is also plotted as a thin curve in Fig. 4(b). In this figure, a constant $\tau_{sf} = 8$ ns (Ref. 18) is assumed for the entire E_{eff} region, and V_{acc} is set to 3 V so that t_e ($= 0.56$ ns) becomes much shorter than τ_{sf}. β_π^{osc} corresponds to β_π, and obeys the universal curve[17] of μ_{eff}. This behavior becomes the crucial evidence of spin transport in the MOS inversion channel. In contrast, when V_{acc} decreases, β_π^{osc} starts to deviate from the universal curve of β_π. This feature is beneficial in attempts to experimentally determine τ_{sf}. Because the dominant scattering mechanisms for μ_{eff} can be changed by E_{eff} (Ref. 17), the relation between the scattering mechanisms and τ_{sf} can be investigated using the presented universality behavior of β_π^{osc}.

[1] S. Sugahara, IEE Proc. Circuits Devices Sys. **152**, 355 (2005).
[2] S. Sugahara, Phys. Status Solidi C **3**, 4405 (2006).
[3] S. Sugahara and J. Nitta, Proc. IEEE **98**, 2124 (2010).
[4] Y. Shuto, R. Nakane, W. H. Wang, H. Sukegawa, S. Yamamoto, M. Tanaka, K. Inomata, and S. Sugahara, Appl. Phys. Express **3**, 013003 (2010).
[5] S. Yamamoto, Y. Shuto, and S. Sugahara, Electron. Lett. **47**, 1027 (2011).
[6] See http://public.itrs.net/ for "The International Technology Roadmap for Semiconductors" (SIA Semiconductor Industry Association, 2009).
[7] B. Huang, D. J. Monsma, and I. Appelbaum, J. Appl. Phys. **102**, 013901 (2007).
[8] B. Huang and I. Appelbaum, Phys. Rev. B **77**, 165331 (2008).
[9] H. J. Jang and I. Appelbaum, Phys. Rev. Lett. **103**, 117202 (2009).
[10] B. Huang and I. Appelbaum, Phys. Rev. B **82**, 241202(R) (2010).
[11] S. P. Dash, S. Sharma, R. S. Patel, M. P. de Jong, and R. Jansen, Nature **462**, 491 (2009).
[12] T. Sasaki, T. Oikawa, M. Shiraishi, Y. Suzuki, and K. Noguchi, Appl. Phys. Lett. **98**, 012508 (2011).
[13] C. H. Li, O. M. J. van 't Erve, and B. T. Jonker, Nat. Commun. **2**, 245 (2011).
[14] M. Tran, H. Jaffrès, C. Deranlot, J.-M. George, A. Fert, A. Miard, and A. Lemaître, Phys. Rev. Lett. **102**, 036601 (2009).
[15] O. M. J. van 't Erve, A. T. Hanbicki, M. Holub, C. H. Li, C. Awo-Affouda, P. E. Thompson, and B. T. Jonker, Appl. Phys. Lett. **91**, 212109 (2007).
[16] Y. Takamura and S. Sugahara, IEEE Magn. Lett. **2**, 3000404 (2011).
[17] S. Takagi, A. Toriumi, M. Iwase, and H. Tango, IEEE Trans. Electron Devices **41**, 2357 (1994).
[18] J. Fabian A. Matos-Abiague, C. Ertler, P. Stano, and I. Zutic, Acta Physica Slovaca **57**, 565 (2007).